

Estimate the Pitch and Heading Mounting Angles of the IMU for Land Vehicular GNSS/INS Integrated System

Qijin Chen^{ID}, Quan Zhang^{ID}, and Xiaoji Niu^{ID}

Abstract—Nonholonomic constraint (NHC) and odometer speed have been proven to significantly improve the navigation accuracy of a global navigation satellite system (GNSS)-aided inertial navigation system (INS) for land vehicular applications. Exploiting the full potential of the NHC and odometer aids requires the inertial measurement unit (IMU) mounting angles, i.e., angular misalignment with respect to the host vehicle, to be precisely known. We address the accurate estimation of the IMU mounting angles through an aided dead reckoning (DR) approach. In this method, DR using the GNSS/INS integrated attitude and distance traveled is fused with the GNSS/INS integrated position through a straightforward Kalman filter. Simulation and field tests are carried out to validate the proposed algorithm for different grade IMUs, including typical navigation-grade, tactical-grade and low-cost IMUs. The results demonstrate that the pitch and heading mounting angles can be estimated with a comparable accuracy with the GNSS/INS attitude solution, for example, 0.001° accuracy can be achieved for a navigation-grade GNSS/INS integrated system. The roll mounting angle can not be estimated due to lack of observability in this approach, and the heading mounting angle estimation may be influenced by the GNSS/INS heading accuracy drift to some extent for the low-cost IMUs.

Index Terms—IMU mounting angle, GNSS/INS integration, dead reckoning(DR), angular misalignment estimation, land vehicle navigation.

I. INTRODUCTION

THE integration of a global navigation satellite system (GNSS) and an inertial navigation system (INS) fully utilizes the advantages of these two subsystems to provide accurate and robust navigation information, including position, velocity and attitude in the open sky, and thus has been extensively applied in civilian vehicular navigation and mobile mapping applications. When traversing areas with a limited sky visibility in urban cities, the GNSS may experience frequent signal interference and outage. Such situations arise

Manuscript received December 24, 2019; revised April 1, 2020 and April 22, 2020; accepted April 28, 2020. This work was supported in part by the National Natural Science Foundation of China under Grant 41904019 and Grant 41674038. The Associate Editor for this article was S. Kong. (*Corresponding author: Xiaoji Niu*)

Qijin Chen is with the GNSS Research Center, Wuhan University, Wuhan 430072, China.

Quan Zhang and Xiaoji Niu are with the GNSS Research Center, Wuhan University, Wuhan 430072, China, and also with the Collaborative Innovation Center of Geospatial Technology, Wuhan University, Wuhan 430079, China (e-mail: xjnu@whu.edu.cn).

Digital Object Identifier 10.1109/TITS.2020.2993052

when a vehicle travels between tall buildings, underneath trees and inside tunnels [1], in which cases the navigation states tend to drift. To maintain an acceptable navigation accuracy and improve the robustness of the system when the GNSS is unavailable, especially for long signal outages, other aiding such as an odometer and nonholonomic constraint (NHC) are introduced. An odometer is a cost-effective and conveniently deployed sensor for civilian land vehicles [2]. NHC refers to the fact that the land vehicle motion is constrained, where the vehicle can only move in the longitudinal direction and the velocity in the plane perpendicular to the longitudinal direction is almost zero [3], [4]. NHC is a kind of virtual velocity observation for a land vehicle, which can be achieved without any additional sensors. Odometers and NHC have been proven to significantly improve the navigation accuracy and enhance the performance of an INS [3], [5], especially when the GNSS signal is unavailable.

The odometer and NHC are the observations valid in the vehicle frame, thus using an odometer or NHC as an aid requires the axes of the inertial measurement unit (IMU) to be aligned with the host vehicle body frame as accurately as possible to exploit their full potential [5], [6]. In practice, an IMU is commonly misaligned with the host vehicle in both position and attitude, which is a common problem for a multisensor integrated system. The position misalignment, known as the lever-arm, can be accurately measured using tape or a total station in advance. The angular misalignment of the IMU with respect to the vehicle body frame, i.e., mounting angles as depicted in Fig. 1, is difficult to measure accurately, which, if ignored or not properly handled, will reduce the benefits of the odometer velocity and NHC updates and even adversely affect the navigation accuracy [5], [7], [8]. Therefore, the present research focuses on the accurate estimation of the IMU mounting angles from the data processing perspective.

A. Related Works

The mounting angle estimation problem has gained attention in previous studies. Studies [5], [6] have pointed out the importance of having knowledge of the IMU mounting angles in using NHC aiding, but an estimation method has not been provided. Hong *et. al* [9], [10] presented car test results for the estimation of the angular misalignment between IMU and global positioning system (GPS) antenna array. In his study,

the angular misalignment between the GPS antenna array and the IMU rather than the IMU mounting angle with respect to the host vehicle was estimated.

Studies [11], [12] have reported utilizing the vehicle acceleration measurement to determine the mounting angles of an IMU or a reduced inertial cluster relative to a land vehicle. The described methods estimated the roll and pitch mounting angles by assuming that the vehicle runs on horizontal road surface with only forward or rearward acceleration, and determined the heading mounting angle based on horizontal accelerations with a known surface orientation. This approach is useful for personal navigation devices or automatic crash notification devices where a 2° accuracy in the yaw-mounting angle estimate can be achieved but is insufficient for some vehicular applications that require high precision mounting angles.

Wu *et al.* [2], [13] addressed the feasibility of an automatic estimation of an inertial sensor/odometer attitude misalignment for land vehicle navigation applications using a NHC and an odometer as a velocity update, and studied the sufficient conditions for the successful self-calibration. Similar applications can be found in [7], [14]–[16]; in [16], [17], the INS/odometer based DR position was utilized in advance as a measurement to integrate with the INS.

Yan [18] studied the error propagation of a dead reckoning (DR) system using an INS and an incremental odometer and found that the uncalibrated pitch and heading mounting angles influenced the DR positioning accuracy significantly for the long-range navigation applications. He pointed out the potential of computing the pitch and heading mounting angle as the DR position errors over the traveled distance. Li *et al.* [19] applied this approach to estimate the mounting angles based on two reference points that have known position coordinates. This method assumes that the mounting angle is the predominant error source causing the DR position drift, which is feasible for a high precision INS, e.g., navigation-grade INS. However, for a low-cost INS, the INS-indicated attitude contains errors comparable in magnitude to the mounting angles, in which case the mounting angle is likely not the dominant error source and the corresponding estimation accuracy may significantly degrade.

We can summarize from the previous studies that the mounting angles were estimated based on acceleration- and velocity-level observations in the navigation states. These methods are based on the fact that if the land vehicle conforms to NHC, the existence of the mounting angles makes the forward or rearward acceleration and velocity have a projection components in the INS-indicated lateral and vertical directions. The results from previous studies shown that the approaches using velocity-level observations has better accuracy than that using acceleration-level measurements. Study [18] inspires us that the IMU mounting angles are expected to be estimated with better accuracy than the existing methods if using position-level observations, e.g., the DR position errors.

B. An Overview of the Proposed Method

The present research proposes a practical approach that can accurately estimate the IMU mounting angles with respect

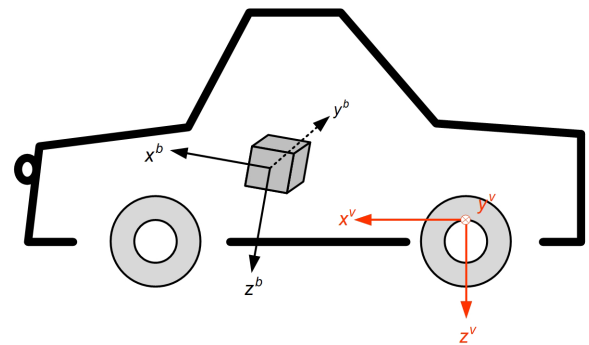


Fig. 1. Illustration of the IMU mounting angles with respect to the host vehicle, and definitions of the vehicle frame (*v*-frame) and IMU body frame (*b*-frame).

to the host land vehicle for different grade land vehicular GNSS/INS systems. Implementation of this method contains two phases, as illustrated in Fig. 2. Phase 1 performs the typical GNSS/INS integration data processing, providing accurate attitude and position solutions to phase 2. Phase 2 estimate the pitch and heading mounting angles through the straightforward Kalman filter (KF) for the aided DR. The remaining sections of this paper is devoted to the algorithm development and testing in phase 2.

This method differs from the previous approaches in the following ways. 1) The mounting angles are estimated through a straightforward KF estimator based on the position error level observations; thus, this method is expected to achieve a better estimation accuracy over the existing approaches. 2) The feasibility and accuracy of the estimation algorithm is evaluated in a real railway track trolley navigation experiment where the reference truth is available, which has been difficult to obtain in previous studies on civilian land vehicles. A numerical simulation and two field tests were carried out to comprehensively evaluate the estimator performance for different-grade GNSS/INS systems. The results demonstrate that the pitch and heading mounting angle estimation converged quickly over a small piece of the trajectory. The pitch and heading mounting angles can be estimated with a comparable accuracy with the GNSS/INS attitude solution, tactical and even low-cost MEMS systems; for example, 0.001° accuracy can be achieved for a navigation-grade GNSS/INS integrated system. The roll mounting angle can not be estimated due to lack of observability in this approach, and the heading mounting angle estimation may be influenced by the GNSS/INS heading accuracy drift to some extent for the low-cost IMUs.

The remainder of this paper is organized as follows: The mounting angle estimation method is described in detail including the implementation details. Then, a numerical simulation and a field test are used to evaluate the proposed method. Details of the simulation and several experiments are described, along with the mounting angle estimation performance. Finally, several important issues regarding this algorithm are discussed, and potential applications are proposed.

II. MOUNTING ANGLE ESTIMATION METHODS

Fig.1 depicts the relation between the host vehicle frame (*v*-frame) and the IMU body frame (*b*-frame). In the *v*-frame,

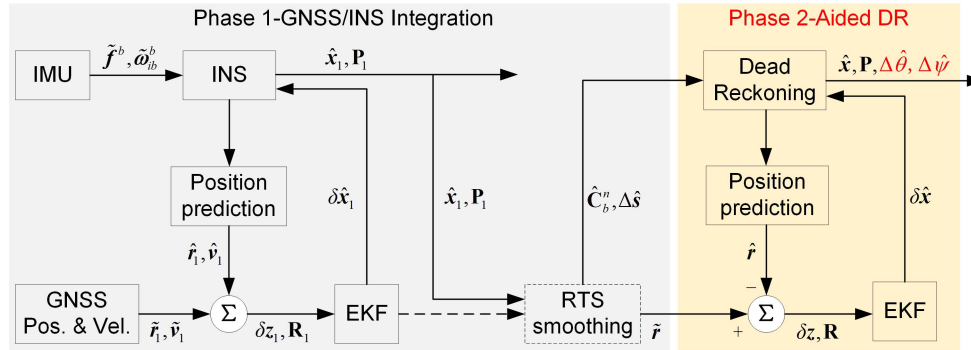


Fig. 2. Block diagram of the IMU mounting angle estimation algorithm.

the x -axis is along the vehicle's forward direction, the z -axis points downward, and the y -axis points outward, in accordance with the right-hand rule. The b -frame roughly aligns with the v -frame in axes with a small misalignment in attitude, i.e., the IMU mounting angles. The IMU mounting angles with respect to the host vehicle are described with a set of Euler angles, denoted by $\Delta\phi$, $\Delta\theta$, and $\Delta\psi$. This representation means that the v -frame is rotated by successive rotation angles $\Delta\psi$, $\Delta\theta$, and $\Delta\phi$ about the z , intermediate y' , and intermediate x'' axes, respectively, to finally align with the b -frame. In this research, the IMU mounting angles are assumed to be small, e.g., smaller than 5° in general. The attitude of a rigid body, e.g., the IMU or vehicle, is defined here as the angular orientation between the rigid body fixed frame and the local level geographic frame (i.e., n -frame, north-east-down).

Fig. 2 shows an overall block diagram of the proposed IMU mounting angle estimation algorithm, which contains two separate phases. Phase 1 performs the GNSS/INS data fusion, whose outputs are used as the inputs of the subsequent phase 2. Note that the choice of a typical loose coupling in phase 1 is completely independent, the GNSS/INS tightly coupled approach is also an alternative. To improve the accuracy of the GNSS/INS integrated solutions, a Rauch-Tung-Striebel (RTS) smoother is applied in data postprocessing utilizing all past, current and future measurements. The RTS smoothing block is plotted by dashed line to indicate that it is suitable for postprocessing and is not mandatory in case the algorithm is applied in the potential real-time situation. We assume that the readers are familiar with the algorithm and implementation of the GNSS/INS data fusion and smoothing, details can be found in [20]–[26]. In the following, we will then focus on developing the IMU mounting angle estimation algorithm in phase 2, as depicted in the right panel of Fig. 2. The source code and a demo for the proposed algorithm are available at <http://dx.doi.org/10.21227-ts0j-3j38>.

A. Mounting Angle Estimation KF

In phase 2, the pitch and heading mounting angles of the IMU are finally estimated through a dedicated extended KF (EKF) using the GNSS/INS integrated solution as the inputs. As illustrated in the right panel of Fig. 2, the GNSS/INS positioning solution is used as the position measurement \tilde{r} for the estimator, and is also used to compute the traveled distance increment vector $\Delta\hat{s}$. The DR performs temporal

update using $\Delta\hat{s}$ and the GNSS/INS attitude $\hat{\mathbf{C}}_b^n$ through the kinematic model to maintain the DR position state \hat{r} . As the DR integrates, the uncertainty in \hat{r} increase due to the existence of IMU mounting angles α , attitude bias, i.e., error in the attitude matrix $\hat{\mathbf{C}}_b^n$, and errors in $\Delta\hat{s}$. The extended KF (EKF) estimator uses the position residual vector $\delta z = \hat{r} - \tilde{r}$ along with the error models to estimate the error state $\delta\hat{x}$, which is fed back into the DR to remove the estimated errors from the system and estimate the mounting angles $\Delta\hat{\theta}$ or $\Delta\hat{\psi}$. Note that $\Delta\phi$ is not estimated due to lack of observability.

For this KF design, the error state vector is defined as

$$\delta x = [\delta r^n, \alpha, \phi, \delta k]^T \quad (1)$$

where

$$\delta r^n = \hat{r}^n - r^n \quad (2)$$

$$\hat{\mathbf{C}}_b^n = [\mathbf{I} - (\phi \times)] \mathbf{C}_b^n \quad (3)$$

$$\hat{\mathbf{C}}_b^v = [\mathbf{I} - (\alpha \times)] \mathbf{C}_b^v \quad (4)$$

where $\delta r^n = [\delta r_N, \delta r_E, \delta r_D]^T$ are the position errors in meter in the directions north, east and down. It is defined as the difference between the DR-indicated position vector \hat{r}^n and true position vector r^n . $\phi = [\phi_r, \phi_p, \phi_h]^T$ represent the biases in GNSS/INS attitude solution in the ϕ -angle formulation [24], [27]. ϕ_r , ϕ_p , ϕ_h denote the error in the roll, pitch and heading angle, respectively. Similarly, $\alpha = [\delta\Delta\phi, \delta\Delta\theta, \delta\Delta\psi]^T$ contains the IMU mounting angle residuals. δk is the scale factor error of the traveled distance measurement. \mathbf{C}_b^n is the b -frame to n -frame transformation matrix. \mathbf{C}_b^v represents the b -frame to v -frame transformation matrix and can be written in terms of the mounting angles by (5), as shown at the bottom of the next page, where c and s refer to the cosine and sine operators, respectively. \mathbf{I} is the 3-by-3 identity matrix. $(\cdot \times)$ denotes the cross-product (skew-symmetric) form of a given 3-D vector. The symbol $\hat{\cdot}$ indicates the variables that contain errors.

In this definition, the GNSS/INS attitude biases are augmented because they induce errors in DR-derived position as derived subsequently. The mounting angle residuals instead of the mounting angles themselves are augmented in order to ensure the adequate linearity of the system model of the KF estimator. It should be noted that $\delta\Delta\phi$ is not augmented due to lack of observability, which will be demonstrated

subsequently. Therefore, 9 elements are contained in the error state vector

$$\delta\mathbf{x} = [\delta r_N, \delta r_E, \delta r_D, \delta\Delta\theta, \delta\Delta\psi, \phi_r, \phi_p, \phi_h, \delta k]^T \quad (6)$$

The filter design requires equations describing the dynamics of the error states. In the following, DR position computation algorithm is introduced, then the dynamics of the error states are derived and discussed in detail.

B. DR Position Computation

The DR position dynamics is described with a set of differential equations of the geographic latitude φ , longitude λ , and height h .

$$\dot{\varphi} = \frac{v_N}{R_M + h} \quad (7)$$

$$\dot{\lambda} = \frac{v_E}{(R_N + h) \cos \varphi} \quad (8)$$

$$\dot{h} = -v_D \quad (9)$$

where R_M and R_N refer to the radii of curvature along lines of constant longitude and latitude, respectively. v_N , v_E , and v_D are the north, east and down components of the velocity resolved in the n -frame \mathbf{v}^n , respectively.

In practice, the vehicle velocity measurement from an odometer is usually referenced to the v -frame, which is then transformed into the n -frame by the following transformation

$$\mathbf{v}^n = \mathbf{C}_b^n \mathbf{C}_v^b \mathbf{v}^v \quad (10)$$

where the vehicle-referenced velocity \mathbf{v}^v has a nonzero value v for the first element (x -/forward component), and the other elements are zeros; i.e., $\mathbf{v}^v = [v, 0, 0]^T$. \mathbf{C}_v^b is the transpose of \mathbf{C}_b^v .

The incremental distance traveled Δs_k^v measured by an odometer or derived from the GNSS/INS trajectory is also referenced to the v -frame and defined as

$$\Delta s_k^v = \int_{t_{k-1}}^{t_k} \mathbf{v}^v(t) dt \quad (11)$$

where t_{k-1} and t_k denotes the discrete time epochs. Δs_k^v also has a nonzero value for the first element (x component) Δs , and the other elements are zeros; i.e., $\Delta s^v = [\Delta s, 0, 0]^T$.

The Cartesian DR position is updated by numerically integrating the geographic velocity components, as

$$\mathbf{r}_k^n = \mathbf{r}_{k-1}^n + \int_{t_{k-1}}^{t_k} \mathbf{C}_b^n(t) \mathbf{C}_v^b(t) \mathbf{v}^v(t) dt \quad (12)$$

where \mathbf{r}_{k-1}^n and \mathbf{r}_k^n are the Cartesian position vector at t_{k-1} and t_k , respectively. In this integration, the mounting angles are generally assumed to be constants; thus, $\mathbf{C}_v^b(t)$ does not change with time. For simplicity, we assume further that the IMU attitude matrix $\mathbf{C}_b^n(t)$ is time-invariant during the

integration interval. This assumption is reasonable as long as the integration period is sufficiently short. Then we have

$$\begin{aligned} \mathbf{r}_k^n &= \mathbf{r}_{k-1}^n + \mathbf{C}_b^n(t_{k-1}) \mathbf{C}_v^b \int_{t_{k-1}}^{t_k} \mathbf{v}^v(t) dt \\ &= \mathbf{r}_{k-1}^n + \mathbf{C}_b^n(t_{k-1}) \mathbf{C}_v^b \Delta s_k^v \end{aligned} \quad (13)$$

In practice, the average of $\mathbf{C}_b^n(t_{k-1})$ and $\mathbf{C}_b^n(t_k)$ instead of $\mathbf{C}_b^n(t_{k-1})$ can also be used in the above equation. We denote

$$\Delta s_k^n = \mathbf{C}_b^n(t_{k-1}) \mathbf{C}_v^b \Delta s_k^v \quad (14)$$

where $\Delta s_k^n = [\Delta s_{N,k}, \Delta s_{E,k}, \Delta s_{D,k}]^T$ denotes the incremental distance traveled resolved in the n -frame.

Therefore, the geographic latitude, longitude and height are updated by numerically integrating (7)~(9) step by step, assuming R_M and R_N are constants in the integration interval.

$$\varphi_k = \varphi_{k-1} + \frac{\Delta s_{N,k}}{R_M + h} \quad (15)$$

$$\lambda_k = \lambda_{k-1} + \frac{\Delta s_{E,k}}{(R_N + h) \cos \varphi} \quad (16)$$

$$h_k = h_{k-1} - \Delta s_{D,k} \quad (17)$$

Equation (15)~(17) are the DR position computation algorithm using the attitude and vehicle-referenced incremental distance measurement, considering the IMU mounting angles.

C. Error State Propagation Model

In the following, we derive the discrete time propagation model of the DR position error and discuss the modeling of the other error states.

1) DR Position Error Model: Equation (13) indicates the DR-indicated position would be imperfect as a result of the initial position error or error in the previous epoch, attitude errors, residual error in the mounting angles after compensation, and distance measurement error. Therefore, in a real case, the computed position is expressed as

$$\hat{\mathbf{r}}_k^n = \hat{\mathbf{r}}_{k-1}^n + \hat{\mathbf{C}}_{b,k-1}^n \hat{\mathbf{C}}_v^b \Delta \hat{s}_k^v \quad (18)$$

The vehicle-referenced incremental distance measurement error is assumed to arise from the scale factor error δk , as

$$\Delta \hat{s}^v = (1 + \delta k) \Delta s^v = \Delta s^v + \Delta s^v \delta k \quad (19)$$

Substituting equations (2)~(4) and (19) into (18), subtracting the true value from the result, and eliminating products of error quantities yields

$$\delta \mathbf{r}_k^n = \delta \mathbf{r}_{k-1}^n - \mathbf{C}_b^n \mathbf{C}_v^b (\Delta s^v \times \boldsymbol{\alpha}) + \Delta s^n \times \boldsymbol{\phi} + \Delta s^n \delta k \quad (20)$$

The expansion of term $\Delta s^v \times \boldsymbol{\alpha}$ can be readily obtained as

$$\Delta s^v \times \boldsymbol{\alpha} = \Delta s \begin{bmatrix} 0 \\ -\delta \Delta \psi \\ \delta \Delta \theta \end{bmatrix} \quad (21)$$

$$\mathbf{C}_b^v = \begin{bmatrix} c \Delta \theta c \Delta \psi & -c \Delta \phi s \Delta \psi + s \Delta \phi s \Delta \theta c \Delta \psi & s \Delta \phi s \Delta \psi + c \Delta \phi s \Delta \theta c \Delta \psi \\ c \Delta \theta s \Delta \psi & c \Delta \phi c \Delta \psi + s \Delta \phi s \Delta \theta s \Delta \psi & -s \Delta \phi c \Delta \psi + c \Delta \phi s \Delta \theta s \Delta \psi \\ -s \Delta \theta & s \Delta \phi c \Delta \theta & c \Delta \phi c \Delta \theta \end{bmatrix} \quad (5)$$

The above equation indicates that the position error is irrelevant to $\delta\Delta\phi$.

Substituting equation (21) into (20) leads to

$$\delta\mathbf{r}_k^n = \delta\mathbf{r}_{k-1}^n - \mathbf{C}_b^n \mathbf{C}_v^b \mathbf{M} \begin{bmatrix} \delta\Delta\theta \\ \delta\Delta\psi \end{bmatrix} + \Delta s^n \times \boldsymbol{\phi} + \Delta s^n \delta k \quad (22)$$

where

$$\mathbf{M} = \begin{bmatrix} 0 & 0 \\ 0 & -\Delta s \\ \Delta s & 0 \end{bmatrix} \quad (23)$$

It is clear from (22) that the pitch and heading mounting angle residuals can be estimated as long as the DR positioning error can be observed with certain accuracy.

2) *Mounting Angle Modeling*: IMU mounting angle modeling is a matter of experience to some extent, since it differs for different applications and depends on the host vehicle condition. For example, when an IMU is rigidly mounted on a railway track trolley without a suspension system, the mounting angles almost do not vary with time and can be treated as constants. In civilian land vehicle applications, the IMU mounting angles are not always constant due to the existence of a vehicle suspension system. The pitch mounting angle, for instance, may vary due to the load, speed and tire pressure. In this case, it is preferable to model the mounting angles as random walks or first order Gauss-Markov process. Furthermore, higher order colored noise may be considered when taking into account the structural deformation for the large scale land vehicles [28]. In practice, for the railway track trolley case, the mounting angles can also be modeled as random walks with intentionally added small noise.

3) *Attitude Error Modeling*: To optimize the KF gain for the aided DR, it is important to match the assumed attitude error model to its true value. However, it is well known that accurately modeling the attitude error of the GNSS/INS solution using an analytical method is too complicated, since the GNSS/INS integrated solution is affected by a variety of error sources, including inertial sensor measurement errors, initialization errors, GNSS positioning errors, and the host vehicle trajectory and dynamics. According to study [29], we choose to approximately model the attitude error as a random walk process. Since an INS integrates measurements from accelerometers and gyroscopes, the white noise components are integrated, which will increase the attitude uncertainty. In practice, a numerical simulation technique can be used to validate the feasibility of the modeling.

4) *Scale Factor Error of the Distance Measurement*: The distance increment for DR computation can be measured by an odometer sensor, derived from GNSS/INS integrated position, or GNSS/odometer integration. For an ordinary civilian vehicle, the scale factor error of the odometer sensor is not constant, and can vary by 1 percent due to changes in the tire pressure, temperature, load and speed [7], [30]. The scale factor error is modeled as a random walk, and the corresponding noise covariance should be tuned in practical applications, which will be discussed later. Notably, in our application, accurate GNSS positions at the centimeter level are assumed to be always available, in which case the scale

factor errors of the odometer measurement can be estimated and compensated accurately prior to the DR positioning. Alternatively, the incremental distance can be derived from the GNSS/INS trajectory, in which case the residual scale factor error is negligibly small. Without loss of generality, the scale factor error of the distance measurement is kept in the state vector of the KF in case the uncompensated incremental distance measurement from an odometer sensor is directly used in DR.

The random walk that we use to model the mounting angles, attitude errors, and the residual distances scale factor, also called a Wiener process, is cumulative sums of a white noise process. The continuous-time state equation for the random walk is given by

$$\dot{x} = w \quad (24)$$

where $E[w(t)w(\tau)] = q(t)\delta(t - \tau)$ [24]; the corresponding discrete-time process is

$$x_{k+1} = x_k + w_k \quad (25)$$

with the noise covariance $q_k = E[w_k w_k^T] = q(t)\Delta t_k$, and Δt_k is the time interval. Details on state modeling and the setting of the process parameters, i.e., the KF system noise covariance tuning, are given later.

5) *Summary of System Model*: Summing up, the mounting angle estimation filter system model in discrete time is given by

$$\delta\mathbf{x}_k = \Phi_{k/k-1}\delta\mathbf{x}_{k-1} + \mathbf{G}_{k-1}\mathbf{w}_{k-1} \quad (26)$$

with $\mathbf{w}_{k-1} \sim N(0, \mathbf{Q}_{k-1})$, Φ denotes the state transition matrix, \mathbf{G} is the discrete time system noise distribution matrix, and \mathbf{w} is the system noise vector. $\Phi_{k/k-1}$, \mathbf{G}_{k-1} , \mathbf{w}_{k-1} are written as

$$\Phi_{k/k-1} = \begin{bmatrix} \mathbf{I}_{3 \times 3} & -\mathbf{C}_b^n \mathbf{C}_v^b \mathbf{M} & (\Delta s^n \times) & \Delta s^n \\ 0 & \mathbf{I}_{2 \times 2} & 0 & 0 \\ 0 & 0 & \mathbf{I}_{3 \times 3} & 0 \\ 0 & 0 & 0 & 1 \end{bmatrix} \quad (27)$$

$$\mathbf{G}_{k-1} = \begin{bmatrix} \mathbf{0}_{3 \times 6} \\ \mathbf{I}_{6 \times 6} \end{bmatrix} \quad (28)$$

$$\mathbf{w}_{k-1} = [w_{\Delta\theta}, w_{\Delta\psi}, w_\phi, w_\theta, w_\psi, w_{SF}]^T \quad (29)$$

where \mathbf{I} refers to the identity matrix; $w_{\Delta\theta}$ and $w_{\Delta\psi}$ are driving noise of the pitch and heading mounting angle models, respectively; w_ϕ , w_θ and w_ψ are the driving noise in the roll, pitch and heading angle models, respectively; w_{SF} is the driving noise of the scale factor error modeling of the distance measurement.

D. Measurement Equations

The measurement sent to the KF estimator is the difference between the DR-indicated position and the GNSS/INS position.

$$\begin{aligned} \delta z_k &= \mathbf{D}(\hat{\mathbf{r}}_k^n - \tilde{\mathbf{r}}_k^n) \\ &= \mathbf{D} \left[\left(\mathbf{r}_k^n + \mathbf{D}^{-1} \delta \mathbf{r}_k^n \right) - \left(\mathbf{r}_k^n - \mathbf{D}^{-1} \mathbf{e}_k \right) \right] \\ &= \delta \mathbf{r}_k^n + \mathbf{e}_k \end{aligned} \quad (30)$$

where $\hat{\mathbf{r}}_k^n$ is the DR-indicated position vector; $\tilde{\mathbf{r}}_k^n$ is the GNSS/INS position vector. $\hat{\mathbf{r}}_k^n$ and $\tilde{\mathbf{r}}_k^n$ are represented in geodetic coordinate, i.e., with a latitude, longitude, and ellipsoid height. \mathbf{D}^{-1} refers to the Cartesian-to-curvilinear position change transformation matrix

$$\mathbf{D}^{-1} = \text{diag} \left(\left[\frac{1}{R_M + h}, \frac{1}{(R_N + h) \cos \varphi}, -1 \right]^T \right) \quad (31)$$

\mathbf{e}_k refers to the measurement noise vector, with $E[\mathbf{e}_k \mathbf{e}_k^T] = \mathbf{R}_k$. \mathbf{R}_k is a 3-by-3 diagonal matrix, and the diagonal elements can be obtained from the error covariance matrix for the position error state of the GNSS/INS solutions.

E. Kalman Filter Tuning

The tuning of the KF involves the selection of values for the system noise covariance matrix, \mathbf{Q}_k , the measurement noise covariance matrix, \mathbf{R}_k , and the initial values of the error covariance matrix, \mathbf{P}_0 . It is important to set and adjust these parameters appropriately to obtain optimal mounting angle estimates from the KF.

In practice, the discrete time system noise matrix \mathbf{Q}_k is a diagonal matrix with

$$\mathbf{Q}_k = \text{diag}([q_{\Delta\theta}, q_{\Delta\psi}, q_\phi, q_\theta, q_\psi, q_{SF}]) \Delta t \quad (32)$$

where $q_{\Delta\theta}$ and $q_{\Delta\psi}$ are the spectral densities of the intentionally added noise in the pitch and heading mounting angle models, respectively. The spectral densities are set with empirical values, usually two orders of magnitude smaller than the value of the gyroscope angular random walk (ARW), so that the mounting angle can be distinguished from the INS attitude uncertainty. q_ϕ , q_θ , and q_ψ are the spectral density of the noise in modeling the attitude errors using a random walk. Simulation results show that they are consistent with the spectral density of the ARW of the gyro outputs, i.e., $q_\phi = q_\theta = q_\psi = ARW^2$. We assumed that the three attitude angles have equal noise characteristics for simplicity. q_{SF} is given an empirical value, and the selection of this value depends on the application conditions, as discussed in the scale factor error modeling. Δt is the average interval between the input of the successive incremental distance and attitude measurement to the DR positioning.

The measurement noise covariance matrix \mathbf{R}_k represents the uncertainty in the GNSS/INS position, which is used as the Kalman filter measurement. Thus, the diagonal elements of \mathbf{R}_k are set with the corresponding element components in the state error covariance matrix, i.e., \mathbf{P} , of the GNSS/INS integration at time epoch k . In Kalman filtering, it is assumed that the measurement errors are uncorrelated; in other words, the measurement noise is white. For the present mounting angle estimation KF, this is not the case, since the input measurement is output by the GNSS/INS smoother. Therefore, we choose to appropriately enlarge the corresponding \mathbf{R} to reduce the gain of the KF [30, p.83].

For the setting of the matrix \mathbf{P}_0 , the elements for the initial DR position and attitude are obtained from the state error covariance matrix, i.e., \mathbf{P} , of the GNSS/INS integration at time epoch k . While the uncertainty of the initial mounting

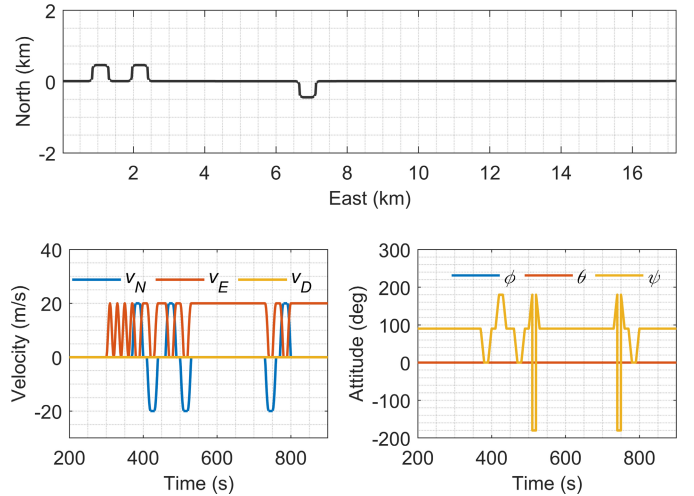


Fig. 3. Simulated trajectory, velocity and attitude of the host vehicle.

angles and scale factor error are set with empirical values. Appropriate empirical values should be given. It is noticeable that an excessively large uncertainty in the initial estimate can sometimes lead to numerical problems [31].

III. SIMULATION

In this section, we use numerical simulations to evaluate the mounting angle estimator performance and discuss the main error sources that influence the accuracy of the mounting angle estimates.

We simulated a land vehicle running on a planar trajectory as depicted in Fig.3, emulating the IMU outputs, GNSS position measurements and corresponding reference data. The onboard IMU is assumed to misalign with the host vehicle frame by $[\Delta\phi, \Delta\theta, \Delta\psi] = [0^\circ, 3^\circ, 2^\circ]$ in attitude, and the origin of the b -frame is assumed without loss of generality to be consistent with that of the v -frame. The GNSS position measurements are generated at 1 Hz and have accuracies of 0.02 m and 0.05 m in the horizontal and vertical directions, respectively, which represent the typical accuracy of the GNSS real-time kinematic positioning mode. The initial attitude of the vehicle is set to 0° , 0° , and 90° for the roll, pitch and heading Euler angles, respectively.

Fig.3 presents the horizontal plane maneuver, velocity and attitude history of the host vehicle, respectively. In the simulation, the vehicle remains stationary for the first 300 s and then runs in a straight line toward east in the following 70 s by alternately accelerating and decelerating with constant accelerations. Then, we keep the vehicle running with a constant speed and alternately change the vehicle's heading clockwise and counter-clockwise to complete a figure-n and figure-u track maneuver and linear alternating acceleration are simulated to improve the observability of the heading errors [2], [9] and accelerate the heading convergence. The vehicle maintains uniform linear motion from 530 s to 730 s, and from 800 s to the end of the simulation.

The IMU outputs are sampled at 200 Hz. Three different error terms are individually added to the perfect inertial sensor

TABLE I
SENSOR ERROR MODELS FOR THE SIMULATED IMUS

	IMU 1	IMU 2	IMU 3
VRW ($m/s/\sqrt{h}$)	0.00075	0.03	0.1
ARW (\deg/\sqrt{h})	0.0022	0.1	0.3
Gyro biases (\deg/h)	$\sigma=0.005$, T=1h	$\sigma=0.25$, T=1000s	$\sigma=40$, T=1000s
Accel. biases (mGal)	$\sigma=25$, T=1h	$\sigma=300$, T=1000s	$\sigma=1000$, T=1000s

outputs to simulate three different grades of IMUs, including a typical high-quality navigation-grade IMU, a tactical-grade IMU, and a low-cost microelectromechanical system (MEMS) IMU. Table I presents the corresponding inertial sensor error models. IMU 1 is the navigation-grade IMU, IMU 2 is a typical tactical-grade IMU, and IMU 3 is a high-grade MEMS IMU. The gyro and accelerometer errors are described by means of constant bias offsets, a white noise process, i.e., an ARW and a velocity random walk (VRW), and a bias variation component described by first-order Gaussian Markov process models characterized by a mean square value σ and correlation time T . Constant offsets are added to the gyroscope and accelerometer outputs to simulate the run-in-run bias, i.e., bias repeatability error, to make the simulated data more realistic. $[0.01, 0.01, 0.01]^{\circ}/h$ is added to IMU1's gyro triads, and $[10, 10, 10]mGal$ is added to the accelerometer triads; $[0.75, -0.5, 0.4]^{\circ}/h$ is added to IMU2's gyro triads, and $[300, 300, 300]mGal$ is added to the accelerometer triads; $[-90, -44, 82]^{\circ}/h$ is added to IMU3's gyro triads, and $[4000, 4000, 4000]mGal$ is added to the accelerometer triads. These values are obtained from real IMUs that have a sensor accuracy comparable to accuracy of the three simulated IMUs. A total of 100 samples are simulated for each IMU to evaluate the estimation repeatability.

The simulated IMU and GNSS position data are first processed to obtain the smoothing navigation solution using the multisensory data fusion software *Cinertial* developed at the Navigation Group at GNSS Research Center, Wuhan University [25]. RTS smoothing was used to improve the accuracy of the integrated navigation solutions. In the fusion of the GNSS and IMU data, the initial positions are given with GNSS position and the velocity is initialized to be zero. The attitude determination, i.e., the alignment, differs for the three IMUs. For IMU 1 and IMU 2, the initial attitude angles are determined by a fine alignment with the stationary data in the first 300 s, and the initial attitude is given for the MEMS IMU. For MEMS IMU 3, the initial constant gyro biases are computed by averaging the outputs of the gyroscopes within the first stationary 300 s and then used as the prior known bias and compensated. This is because the Earth's rotation rate ($\approx 15^{\circ}/h$) is negligibly small with respect to the large biases of the gyroscopes of $100^{\circ}/h$ [21]. Notably, in the GNSS/INS integration, a NHC has not been used. The GNSS/INS smoothing solution from 800 s to the end of the simulation are then used as inputs to the mounting angle KF estimator, i.e., the second phase as depicted in Fig.2, because the heading converges after the maneuver in the first 800 s.

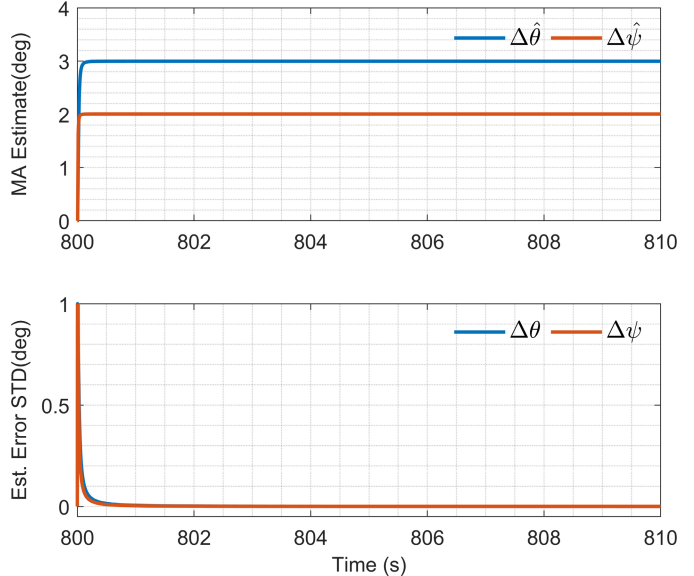


Fig. 4. Mounting angle (MA) estimates for IMU 1. The top graph shows the estimated pitch and heading mounting angles. The bottom graph shows the standard deviation of the mounting angle estimation errors. (Only the first ten seconds are plotted).

In the subsequent mounting angle estimation KF in the second phase, the initial position for DR is read from the GNSS/INS smoothing trajectory, and the mounting angles are initialized with zeros. For the initial state error covariance matrix, i.e., \mathbf{P}_0 , the position and attitude angle uncertainties are read from the state error covariance matrix, i.e., \mathbf{P} , of the aided INS smooth solution. The uncertainties of the entered initial mounting angle and odometer scale factor are set as 1° and 1000 ppm, respectively.

The estimation results for the 100 simulation samples are quite consistent with each other for each IMU, and the results of one typical sample are presented below. Fig.4 plots the mounting angle estimates and its corresponding estimation error variance from IMU 1. The results show that the estimation converges quickly, e.g., within several seconds; thus, only the first 10 s are plotted. The situation for IMU2 and IMU 3 are quite similar. Fig.5 compares the estimated mounting angles with the reference truth value and plots the deviation of the parameter estimates. The result shows that pitch mounting angle estimation errors are within 0.005° for the three different IMU cases. The estimation error plots seem quite stable. The results are similar for the heading mounting angle, but there is a small offset in the $\Delta\psi$ estimate for IMU 3. This is because in DR, the mounting angles are indistinguishable from the offset in the attitude angle used as the input for the mounting angle estimation. This result can be validated from the heading errors of the GNSS/INS integrated solution as depicted in Fig.6.

Fig.6 shows that the heading angles of the GNSS/INS smoothing solution contain an offset of approximately 0.04° and an obvious drift for IMU 3. Because the simulated vehicle maintains uniform linear motion in this segment, i.e., from 800 s to 1200 s, the heading error is unobservable and tends to drift. The offset component may arise from the residual bias after convergence. Since the mounting angle is indistinguishable

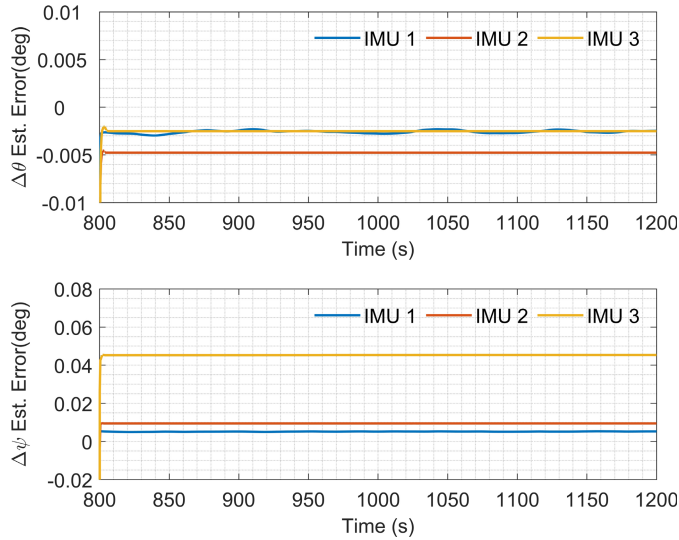


Fig. 5. Error of the mounting angle estimates from the three simulation cases.

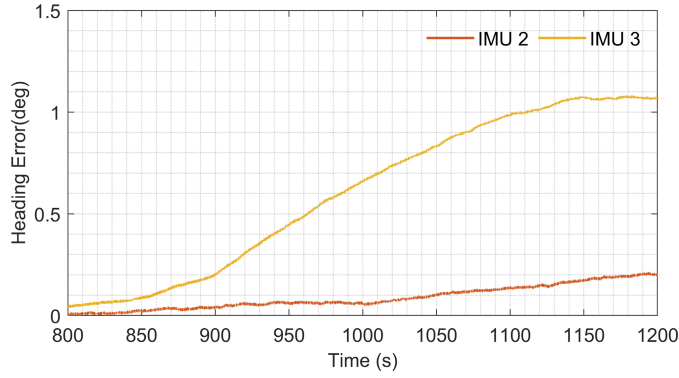


Fig. 6. GNSS/INS heading errors.

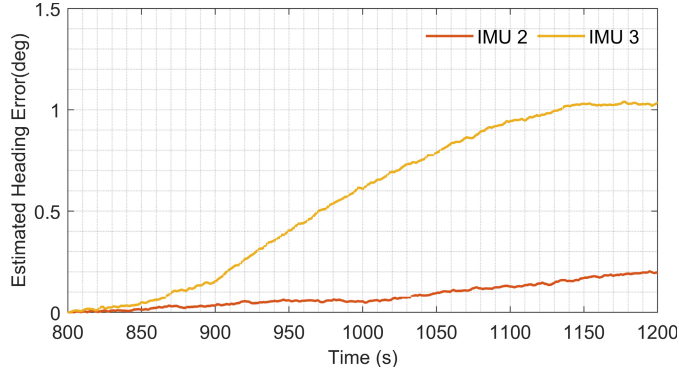


Fig. 7. The estimated heading errors in the mounting angle estimation KF.

with constant attitude biases, the constant component of the attitude error will be mistaken as the mounting angles by the parameter estimation KF. The heading drift seems to have no significant effect on the estimation, because the characteristics of the mounting angles and attitude drift are quite different and distinguishable, and the KF can estimate the attitude errors to some extent.

Fig. 7 shows the estimated heading errors from the parameter estimation KF. Comparing Fig. 6 and Fig. 7, we find that the

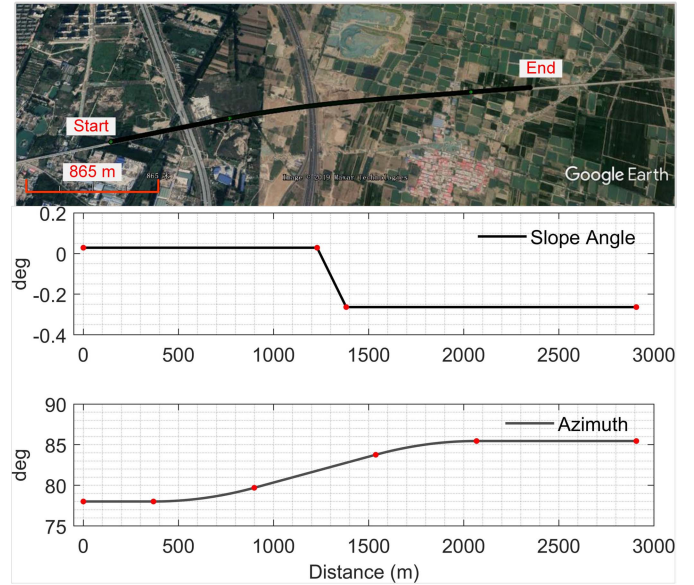


Fig. 8. Field test route (upper, from Google Earth), nominal slope angle and azimuth of the track (lower) with red dots label the intersection points between different type track segments.

heading drift component can be estimated with satisfactory accuracy, while this KF cannot estimate the constant offset in the heading errors.

IV. FIELD TESTS

An advantage of the simulation approach is availability of the ground truth, which is a challenge for most civilian vehicular navigation applications. In this section, the performance of the proposed algorithm is assessed using a railway track trolley running on a high speed railway track, in which case the reference truth can be obtained too. Then we validate the feasibility of the mounting angle estimator in real land vehicular navigation application.

A. Rail Trolley Positioning Applications

A railway track geometry measuring trolley (TGMT) is a special vehicle that differs from civilian land vehicles since it cannot change its course arbitrarily. It is able to keep rigid contact with the rails when moving on the track, and conforms to NHC quite well even when small railway track deformation exist. More details can be found in [32], [33]. For a high-speed railway track, the designed nominal geometric parameters, including the position coordinates, bank, slope, and azimuth angles along the track can be calculated given a mileage [34]. As long as the track is sufficiently accurate, the host trolley vehicle's "true" attitude can be obtained from the nominal track bank, slope and azimuth angles. For illustration, Fig. 8 depicts the nominal slope angle and azimuth versus the mileage of the surveyed track.

The test was carried out on a newly-built high-speed line in central China. The rails had been adjusted to millimeter accuracy according to the construction requirement, which is sufficiently accurate for our evaluation. Fig. 9 shows a

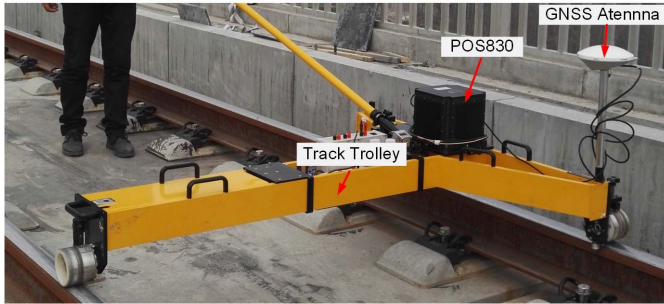


Fig. 9. Photograph of the experiment setup.

photograph of the track trolley. A navigation-grade GNSS/INS integrated system, POS830, from Beijing NAV Technology Co., Ltd, Beijing, China, is used. It integrates a high-precision ring laser gyro (RLG) triad, a high-stability quartz accelerometer triad, and a GNSS OEM6 card from NovAtel Inc., Calgary, Alberta, Canada. The IMU and built-in GNSS receiver are sampled at 200 Hz and 1 Hz, respectively. The IMU has comparable performance with IMU 1 in Table I. A GNSS base station recorded simultaneously at 1 Hz was set up nearby to allow for carrier phase based differential GNSS positioning processing. The baseline length between the rover receiver and base station does not exceed 5 km. Since the surveyed rail segment is in a fully open sky environment, the GNSS receivers had fairly favorable observation circumstances.

The test lasted 50 minutes, and the trolley remained stationary for the first 10 minutes for a static fine alignment. The GNSS data were postprocessed in carrier phase based differential mode to provide centimeter accuracy positions and then fused with the IMU data in a loosely coupled architecture with the same configuration as in the simulation analysis. The data was processed iteratively using the heading estimate and the corresponding uncertainty from the previous processing step as the initial value for the next iteration to eliminate the possible constant offset component in the initial heading. In the parameters estimation KF, small system noise with spectral density of $1.0\text{e-}4^\circ/\sqrt{\text{Hz}}$ was intentionally added to the mounting angle states to model as a random walk.

Fig.10 depicts the difference between the GNSS/INS-indicated IMU attitude and the trolley attitude derived from the nominal track geometric parameters. This angular difference comprises the attitude error in GNSS/INS integration, attitude deviation due to the small track deformation, and the mounting angle. The attitude angles are known accurate to 0.001° for the navigation-grade POS830 in postprocessing. The millimeter level rail deformation tends to cause zero-mean attitude errors [32]. Therefore, the significant offsets in the difference series can be interpreted as the actual (reference truth) pitch and heading mounting angles of the IMU, average of which are -0.345° and 0.845° for the pitch and heading, respectively.

Fig.11 shows that the pitch and heading mounting angle estimates converges quickly in approximately 10 s, and the plot remains stable after 200 s. The estimated pitch and heading mounting angles are -0.344° , 0.844° , respectively, which can

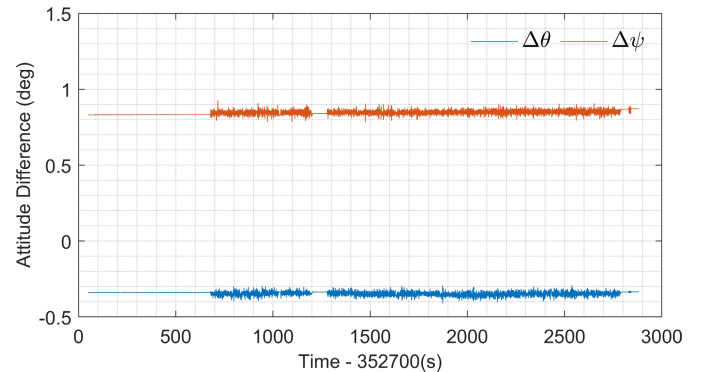


Fig. 10. Difference between the IMU attitude angles and the nominal trolley attitude.

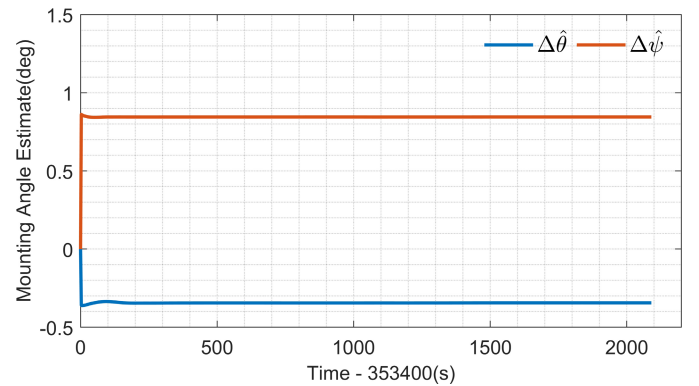


Fig. 11. Mounting angle estimate.

be readout from the plots in this figure. It demonstrates that the mounting angle estimates are accurate to 0.001° , which has the identical accuracy with the GNSS/INS smoothing attitude.

B. Land Vehicle Navigation Applications

Data from a land vehicle test conducted in Wuhan on Jan. 11, 2018 was used to evaluate the feasibility of the proposed method for land vehicular navigation applications. Fig.12 shows a photograph of the vehicle and the system setup. In this test, three different grades GNSS/INS integrated systems were used, including a navigation-grade system POS-A15, a typical tactical-grade system POS-320, and a low-cost MEMS-grade system INS-Probe. POS-A15, POS-320 and INS-Probe have identical inertial sensor specification parameters to the IMU 1, 2 and 3 as listed in Table I. INS-Probe is developed out group. It integrates a MEMS IMU, ADI16465, from Analog Devices Inc. (ADI), MA, USA, and a ZED-F9P high-precision GNSS module from u-blox, Thalwil, Switzerland.

Fig. 13 shows the driving path, which is in a fully open sky condition. The vehicle ran such a complicated trajectory to accelerate the integrated state convergence. A GNSS base station was set nearby and recorded raw observations simultaneously at 1 Hz. The GNSS and IMU data were processed in the same manner with a similar configuration as in the railway trolley test. Odometer speed measurement and NHC were not used, even the odometer data were recorded in the experiment. The data contains a stationary period of 400 s



Fig. 12. Photograph of the field test vehicle and system setup inside the vehicle.



Fig. 13. Trajectory of the vehicular navigation test (labeled with green dot, From Google Earth).

at the beginning, allowing for a static fine alignment for the POS-A15. The initial heading for POS-320 and INS-Probe were obtained from POS-A15 heading angle solution.

Fig.14 depicts the pitch and heading mounting angle estimates for the POS-A15, POS320 and the INS-Probe, respectively. It indicates the estimation converges quickly in approximately 20 s for the navigation- and tactical-grade systems. The situation for the MEMS INS-Probe is slightly different: the estimation can also converge quickly, but the estimates curve is not as stable as those for POS-A15 and POS320. This result can be explained by the fact that the low-cost MEMS GNSS/INS system has larger heading errors, which influence the estimation accuracy of the mounting angles, as discussed in the simulation. It should be noted that three IMUs have their own mounting angles with respect to the host vehicle, thus the difference in the estimate values are not the difference in accuracy.

In the field test, the IMUs were roughly aligned with the vehicle axes, but there is no easy way to accurately measure the misalignment angles of the IMU with respect to the host vehicle to provide reference truth. As proposed by Wu *et al.* [13], the correctness of the estimation can be validated by checking the history of the velocity revolved in the v -frame. If the mounting angles are correct, then there should be no significant velocity component in the lateral and vertical directions of the v -frame.

Fig. 15 shows the integrated velocity from INS-Probe resolved in the b -frame, denoted by v^b , and v -frame, denoted by v^v . In the upper panel, an apparent offset in v_y^v can be observed due to the existence of the mounting angles. As

comparison, this offset vanishes in v_y^v after applying the pitch and heading mounting angle estimates. The velocity offset in the vertical direction is not so significant as depicted in the lower panel, because the pitch mounting angle is small to 0.26°. This indirectly and partially validates feasibility of the estimated parameters. It should be noted that the same conclusions can also be drawn from the results of POS-A15 and POS-320.

V. DISCUSSION

Comparing the results from the simulation and the field tests, two facts are noticed. 1) Simulation results seems to be more accurate in the estimation of the mounting angles, especially for the low-grade IMU. The result for the railway track trolley test is in better agreement with the simulation case than the ordinary land vehicle case. 2) For the low-grade IMU, the mounting angle estimates change slightly if different segments of the trajectory, namely, different time periods, are used. Here, a question arises corresponding to this phenomenon: *"what are the dominant error sources that influence the estimation accuracy, and how can one ensure the estimation performance in practice?"*.

In the simulation, the IMU is attached to the vehicle as an ideal rigid body, where the IMU mounting angles remain perfectly unchanged. In a real field test, for a consumer land vehicle in particular, the IMU mounting angles tend to vary slightly due to the vehicle condition, as discussed in section II. Thus, in real land vehicular applications, the IMU mounting angle is suggested to be modeled as random walk by intentionally adding some noise to the state to absorb the actual variation in the mounting angles.

The mounting angle estimator contains a DR procedure based on the GNSS/INS attitude and increment distance measured in the v -frame. Such a DR procedure assumes that the host vehicle necessarily conforms to the NHC exactly. If the NHC condition is violated, additional error is introduced into the DR computation. In the simulation case, the vehicle is simulated as a mass point and ideally conforms to the NHC condition. However, for a civilian land vehicle, the NHC is somewhat violated due to the presence of slight side slip during cornering and vibrations caused by the engine and suspension system [3]. An NHC violation is much more insignificant for the trolley case, since the track trolley does not have a suspension system and is governed strictly by the rails when moving on rails. This can explain why the results for the railway test are closer to the simulation cases.

Therefore, for consumer land vehicle navigation applications, a straight-line trajectory is suggested for the post-calibration of the IMU mounting angle to minimize the NHC violation as the vehicle turns around. In addition, the NHC condition is more preferable at the center of the rear axle of the vehicle than at other points of the vehicle; thus, the GNSS/INS smoothing position is suggested to be projected to that point in the first phase. The influence of the lever arm when using an NHC in civilian vehicle navigation is studied in a companion research.

It is obvious from equation (22) that the attitude error influences the DR position and further affects the mounting angle

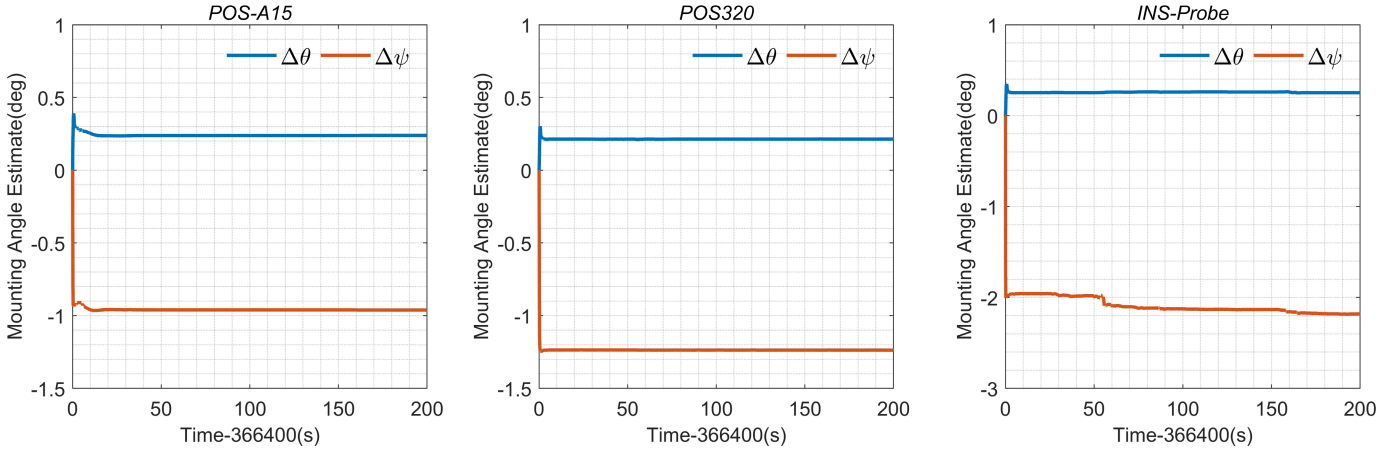


Fig. 14. Estimated mounting angles of the three IMUs with respect to the host vehicle.

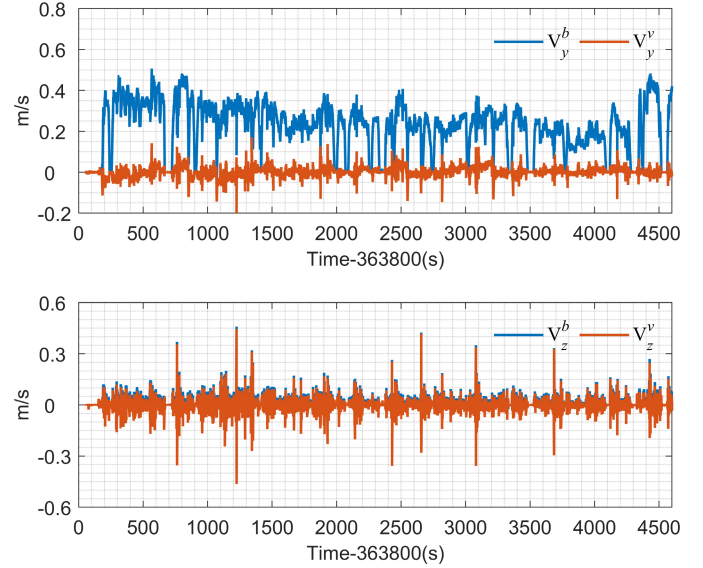
estimation accuracy. The mounting angle estimator cannot distinguish the real IMU mounting angle from the constant bias in the attitude angle readings from the GNSS/INS solutions. This is why the estimate of the mounting angles changes slightly when a different segment trajectory is selected, since for the MEMS IMU, the attitude angles may contain different constant biases in different periods. The attitude drift can be separated from the IMU mounting angle to some extent.

Therefore, to enhance the IMU mounting angle estimation, it is necessary to ensure that the GNSS/INS attitude is as accurate as possible. There are several approaches that can be used to improve the attitude accuracy and include the following.

- The vehicle is suggested to drive with a changing horizontal acceleration to improve the observability of the heading error and accelerate the heading accuracy convergence. Zero velocity update is suggested to use to improve the roll and pitch accuracies when the vehicle stops.
- The fusion of the GNSS and IMU data can be processed iteratively using the parameter estimates and the associated uncertainties as initial values and standard deviations (STD) from the previous iteration during postprocessing [11], [18].
- A trajectory in a fully open sky environment is suggested to ensure that the carrier phase differential GNSS is available.
- Dual-antennas or multi-antenna arrays can be used if possible to improve observability and accuracy of the GNSS/INS heading [28], especially for the low-cost MEMS systems.

It should be noted that for GNSS and IMU data fusion in the phase 1, an NHC observation should not be used, because the utilization of an NHC would lead to the INS's attitude converging to the vehicular attitude.

In the proposed method, the IMU mounting angles are assumed to be small angles, e.g., smaller than 5°, as in previous research. Thus the IMU is suggested to mount roughly align with the host vehicle. If large mounting angles exist, an axis adjustment should be applied to the IMU data prior to data processing. In the present research, the roll mounting angle is unobservable, as reported by other researchers in DR. The

Fig. 15. GNSS/INS integrated velocity history from INS-Probe resolved in the b -frame and the v -frame. Subscripts y and z indicate the lateral and vertical direction, respectively.

roll mounting angle has little influence on the DR navigation accuracy and can be calibrated by stopping the vehicle on a horizontal place to roughly compute the roll mounting angle, as suggested in [11], so as to complete the estimation of the three mounting angles.

VI. CONCLUSION

Accurate knowledge about the IMU mounting angles with respect to the host vehicle is required to exploit the fullest potential of the NHC and odometer aiding. In the present research, we proposed a new method to achieve an accurate estimation of the IMU mounting angles. The implementation of this method contains two separate phases, where the outputs of phase 1 are used as the inputs of phase 2. Phase 1 is a typical implementation of a GNSS/INS integration. In phase 2, a DR positioning procedure is implemented using the obtained attitude and the incremental distance derived from the position solution. The mounting angles are

estimated through a dedicated straightforward KF estimator for DR aided by GNSS/INS position. The source code and a demo for the proposed algorithm are available at <http://dx.doi.org/10.21227/7s0j-3j38>.

Both a numerical simulation and two field tests were performed to evaluate the estimator performance. The results showed that the pitch and heading mounting angle estimation converged quickly over a small piece of the trajectory. The mounting angle for a navigation-grade GNSS/INS system can be estimated to 0.001° accuracy in both simulation and field tests. The estimator cannot distinguish the mounting angle and the attitude offsets; therefore, the estimation accuracy for tactical and low-cost MEMS systems may be affected by biases in the GNSS/INS attitude solution. The estimator is immune to the time-varying component of the drift in the GNSS/INS smoothing attitude to some extent. Once the attitude bias is minimized, the IMU mounting angles are expected to be estimated with a comparable accuracy to the accuracy of the GNSS/INS smoothing attitude for navigation, tactical and even low-cost MEMS systems.

One potential interesting application of the estimation method is an accurate system-level calibration of the IMU mounting angle for a railway TGMT system and for a long-range vehicular INS/odometer navigation system, which requires accurate mounting angles. This method can also be used to estimate the relative attitude misalignment between two IMUs mounted on the same vehicle by using the v-frame as the intermediate frame. Accurate estimates of the IMU mounting angles would enhance the benefit of NHC and odometer speed measurement in improving the navigation performance, especially during GNSS signal outage.

ACKNOWLEDGMENT

The authors would like to thank Dr. Hailiang Tang in our group for providing the INS-Probe in the vehicle field test. The authors would also like to thank Kai Yi and Lingkan Zeng within Wuhan MAP Space Time Navigation Technology Company, Ltd for their support in the land vehicle test.

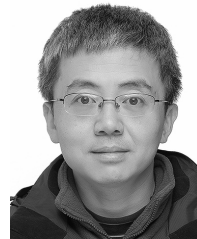
REFERENCES

- [1] C. R. Carlson, J. C. Gerdes, and J. D. Powell, "Error sources when land vehicle dead reckoning with differential wheelspeeds," *Navigat., J. Inst. Navigat.*, vol. 51, no. 1, pp. 13–27, Mar. 2004.
- [2] Y. Wu, M. Wu, X. Hu, and D. Hu, "Self-calibration for land navigation using inertial sensors and odometer: Observability analysis," in *Proc. AIAA Guid., Navigat., Control Conf.*, Aug. 2009, p. 5970.
- [3] G. Dissanayake, S. Sukkarieh, E. Nebot, and H. Durrant-Whyte, "The aiding of a low-cost strapdown inertial measurement unit using vehicle model constraints for land vehicle applications," *IEEE Trans. Robot. Autom.*, vol. 17, no. 5, pp. 731–747, Oct. 2001.
- [4] S. Sukkarieh, "Low cost, high integrity, aided inertial navigation systems for autonomous land vehicles," Ph.D. dissertation, Dept. Mech. Mechatron. Eng., Univ. Sydney, Sydney, NSW, Australia, 2000.
- [5] Z. F. Syed, P. Aggarwal, X. Niu, and N. El-Sheimy, "Civilian vehicle navigation: Required alignment of the inertial sensors for acceptable navigation accuracies," *IEEE Trans. Veh. Technol.*, vol. 57, no. 6, pp. 3402–3412, Nov. 2008.
- [6] X. Niu and S. Han, "Improving the performance of portable navigation devices by using partial IMU based GPS/INS integration technology," in *Proc. ION GNSS*, 2008, pp. 232–238.
- [7] W. Jia, X. Xiao, and Z. Deng, "Self-calibration of INS/Odometer integrated system via Kalman filter," in *Proc. IEEE 5th Int. Conf. Adv. Comput. Intell. (ICACI)*, Oct. 2012, pp. 224–228.
- [8] X. Zhi and P. V. W. Loomis, "Navigation sensor mounting-angle calibration," U.S. Patent 8433514, Apr. 30, 2013.
- [9] S. Hong, M. H. Lee, H.-H. Chun, S.-H. Kwon, and J. L. Speyer, "Experimental study on the estimation of lever arm in GPS/INS," *IEEE Trans. Veh. Technol.*, vol. 55, no. 2, pp. 431–448, Mar. 2006.
- [10] S. Hong, M. H. Lee, S. H. Kwon, and H. H. Chun, "A car test for the estimation of GPS/INS alignment errors," *IEEE Trans. Intell. Transp. Syst.*, vol. 5, no. 3, pp. 208–218, Sep. 2004.
- [11] E. Vinande, P. Axelrad, and D. Akos, "Mounting-angle estimation for personal navigation devices," *IEEE Trans. Veh. Technol.*, vol. 59, no. 3, pp. 1129–1138, Mar. 2010.
- [12] R. C. McKown, "Mounting angle calibration for an in-vehicle accelerometer device," U.S. Patent 9599633, Mar. 21, 2017.
- [13] Y. Wu, C. Goodall, and N. El-Sheimy, "Self-calibration for IMU/odometer land navigation: Simulation and test results," in *Proc. ION Int. Tech. Meeting*, vol. 2, 2010, pp. 1009–1019.
- [14] K. Tang, J. Wang, W. Li, and W. Wu, "A novel INS and Doppler sensors calibration method for long range underwater vehicle navigation," *Sensors*, vol. 13, no. 11, pp. 14583–14600, 2013.
- [15] B. V. Klimkovich, "Self-calibration of a digital odometer integrated with a three-component SINS for a land vehicle," in *Proc. 24th Saint Petersburg Int. Conf. Integr. Navigat. Syst. (ICINS)*, May 2017, pp. 1–4.
- [16] C. Zhao, Y. Qin, and G. Yan, "On-the-move alignment for strapdown inertial navigation system," in *Proc. IEEE Int. Conf. Inf. Autom.*, Jun. 2008, pp. 1428–1432.
- [17] Q. Wang, M. Fu, X. Xiao, and Z. Deng, "Automatic calibration and in-motion alignment of an odometer-aided INS," in *Proc. Chin. Control Conf.*, 2012, pp. 2024–2028.
- [18] G. Yan, "Research on autonomous position and azimuth determining systems for land vehicles," Ph.D. dissertation, School Autom., Northwestern Polytech. Univ., Xi'an, China, 2006.
- [19] Q. Li, Z. Chen, Q. Hu, and L. Zhang, "Laser-aided INS and odometer navigation system for subway track irregularity measurement," *J. Surv. Eng.*, vol. 143, no. 4, Nov. 2017, Art. no. 04017014.
- [20] P. Teunissen and O. Montenbruck, *Springer Handbook of Global Navigation Satellite Systems*. Cham, Switzerland: Springer, 2017.
- [21] E.-H. Shin, "Estimation techniques for low-cost inertial navigation," Ph.D. dissertation, Dept. Geomatics Eng., Univ. Calgary, Calgary, AB, Canada, 2005.
- [22] P. G. Savage, "Strapdown inertial navigation integration algorithm design part 1: Attitude algorithms," *J. Guid., Control, Dyn.*, vol. 21, no. 1, pp. 19–28, Jan. 1998.
- [23] P. G. Savage, "Strapdown inertial navigation integration algorithm design part 2: Velocity and position algorithms," *J. Guid., Control, Dyn.*, vol. 21, no. 2, pp. 208–221, Mar. 1998.
- [24] R. M. Rogers, *Applied Mathematics in Integrated Navigation Systems*, 3rd ed. Reston, VA, USA: AIAA, 2007.
- [25] X. Niu *et al.*, "Development and evaluation of GNSS/INS data processing software for position and orientation systems," *Surv. Rev.*, vol. 47, no. 341, pp. 87–98, Mar. 2015.
- [26] J. F. Wagner and T. Wieneke, "Integrating satellite and inertial navigation-conventional and new fusion approaches," *Control Eng. Pract.*, vol. 11, no. 5, pp. 543–550, 2003.
- [27] D. Titterton and J. L. Weston, *Strapdown Inertial Navigation Technology*, 2nd ed. Stevenage, U.K: IET, 2004.
- [28] J. F. Wagner and G. Kasties, "Applying the principle of integrated navigation systems to estimating the motion of large vehicles," *Aerospace Sci. Technol.*, vol. 8, no. 2, pp. 155–166, Mar. 2004.
- [29] Q. Zhang, X. Niu, Q. Chen, H. Zhang, and C. Shi, "Using allan variance to evaluate the relative accuracy on different time scales of GNSS/INS systems," *Meas. Sci. Technol.*, vol. 24, no. 8, Aug. 2013, Art. no. 085006.
- [30] P. D. Groves, *Principles of GNSS, Inertial, and Multisensor Integrated Navigation Systems*. Boston, MA, USA: Artech House, 2008.
- [31] R. G. Brown and P. Y. C. Hwang, *Introduction to Random Signals and Applied Kalman Filtering: With MATLAB Exercises*, 4th ed. Hoboken, NJ, USA: Wiley, 2012.
- [32] Q. Chen, X. Niu, Q. Zhang, and Y. Cheng, "Railway track irregularity measuring by GNSS/INS integration," *Navigation*, vol. 62, no. 1, pp. 83–93, Mar. 2015.
- [33] Q. Chen *et al.*, "A railway track geometry measuring trolley system based on aided INS," *Sensors*, vol. 18, no. 2, p. 538, 2018.
- [34] W. Schofield and M. Breach, *Engineering Surveying*, 6th ed. Boca Raton, FL, USA: CRC, 2007.



Qijin Chen received the B.Eng. and Ph.D. degrees in geodesy and survey engineering from Wuhan University, Wuhan, China, in 2011 and 2016, respectively.

He is currently a Post-Doctoral Fellow with the GNSS Research Center, Wuhan University. His research interests include INS with aiding and its applications in geodesy and precise surveying engineering, including railway track geometry measuring and underground pipeline surveying.



Xiaoji Niu received the bachelor's and Ph.D. degrees from the Department of Precision Instruments, Tsinghua University, in 1997 and 2002, respectively.

He did Post-Doctoral Research with the University of Calgary and worked as a Senior Scientist at SiRF Technology Inc. He is currently a Professor with the GNSS Research Center, Wuhan University, China. He has published more than 90 academic articles and own 28 patents. He leads a multisensor navigation group focusing on GNSS/INS integrations, low-cost navigation sensor fusion, and its new applications.



Quan Zhang received the B.S. degree in geomatics engineering from the Shandong University of Science and Technology in 2009 and the Ph.D. degree from Wuhan University in 2015.

From 2017 to 2018, he was a Post-Doctoral Researcher with the Digital Photogrammetry Research Group (DPRG), Lyles School of Civil Engineering, Purdue University. He is currently a Research Assistant and a Post Doctor with the GNSS Research Center and the Collaborative Innovation Center of Geospatial Technology, Wuhan

University. His research interests include the inertial navigation and the GPS/INS integration technology.